First Observations of Seasonal Variability in Water Mass Properties Across the Agulhas Current

Laura Braby, Julie Deshayes, Lisa Beal, Tamaryn Morris, Guillaume Novelli, James Maitland, Isabelle J. Ansorge, Juliet Hermes

▶ **To cite this version:**

Laura Braby, Julie Deshayes, Lisa Beal, Tamaryn Morris, Guillaume Novelli, et al.. First Observations of Seasonal Variability in Water Mass Properties Across the Agulhas Current. Journal of Geophysical Research. Oceans, 2022, 127 (9), 10.1029/2021jc018107 . hal-03811159

HAL Id: hal-03811159
https://hal.science/hal-03811159

Submitted on 12 Oct 2022

HAL is a multi-disciplinary open access archive for the deposit and dissemination of scientific research documents, whether they are published or not. The documents may come from teaching and research institutions in France or abroad, or from public or private research centers.

L'archive ouverte pluridisciplinaire **HAL**, est destinée au dépôt et à la diffusion de documents scientifiques de niveau recherche, publiés ou non, émanant des établissements d'enseignement et de recherche français ou étrangers, des laboratoires publics ou privés.

Distributed under a Creative Commons Attribution 4.0 International License

Check for updates

JGR Oceans

RESEARCH ARTICLE
10.1029/2021JC018107

First Observations of Seasonal Variability in Water Mass Properties Across the Agulhas Current

Laura Braby[1,2], Julie Deshayes[3], Lisa Beal[4], Tamaryn Morris[1,5], Guillaume Novelli[4], James Maitland[2,6], Isabelle Ansorge[2], and Juliet Hermes[1,2,7]

[1]South African Environmental Observation Network- Egagasini Node, Cape Town, South Africa, [2]Department of Oceanography, University of Cape Town, Cape Town, South Africa, [3]LOCEAN-IPSL, Sorbonne Universités-CNRS-IRD-MNHN, Paris, France, [4]Rosenstiel School of Marine and Atmospheric Sciences, University of Miami, Miami, FL, USA, [5]South African Weather Service, Marine Unit, Cape Town, South Africa, [6]South African Environmental Observation Network- uLwazi Node, Cape Town, South Africa, [7]Nelson Mandela University, Port Elizabeth, South Africa

Abstract The seasonal variability of Agulhas Current properties is not well understood because there have been few data collected during austral winter. Here we analyze 8 repeat hydrographic sections that have been collected across the Agulhas Current at 34°S over the past decade, including the first full-depth winter surveys of the Agulhas Current, collected in 2016 and 2018. Several differences between the summer and winter occupations of the current are observed which can be attributed to seasonal variability. The most significant difference is the upward shoaling of central waters onto the continental shelf in the summer. These waters flood the shelf with nutrients and oxygen during the summer months, when the Agulhas Current is strongest, but not during winter. Over the top 100 m of the water column seasonality is dominated by surface fluxes, with warmer waters in summer. Immediately below the surface, however, waters are warmer during winter because of the mixing down of Tropical Surface Waters into the deepening mixed layer. Throughout the Agulhas Current at central and intermediate depths waters are cooler in summer and this is due to the upward tilt of the isopycnals, consistent with stronger geostrophic transport. Seasonality is also evident at depth, where North Atlantic Deep Water has a stronger equatorward flow during winter when the Agulhas Current is weaker and shallower.

Plain Language Summary Seasonal changes in temperature and salinity across the Agulhas Current are not well understood because there have been limited hydrographic data collected in this region during winter. In this study, we use a decade worth of observations over the same transect of the Agulhas Current at 34°S, including the first two full-depth winter surveys of the Agulhas Current, to investigate any changes in the water masses properties from one season to another. In summer, when the Agulhas Current is stronger, nutrient-rich water masses located offshore and at depth are observed to migrate upward onto the continental shelf, a phenomenon that is not apparent during winter. The upper part of the Agulhas Current is influenced by surface fluxes, with warmer temperatures occurring during summer. Below the surface layer, Agulhas Current temperatures are cooler during summer as a result of the upward tilt of the density surfaces in association with the stronger current. In winter, when the Agulhas Current is relatively weaker and shallower than in summer, we observe more equatorward flow of the deepest water mass, that is North Atlantic Deep Water.

Key Points:

- Nutrient-rich central waters upwell onto the continental shelf during summer, when the Agulhas Current is stronger, and not during winter
- Below the seasonal surface layer, waters in the Agulhas Current are cooler during summer due to the upward tilt of isopycnals
- More equatorward flow of North Atlantic Deep Water is observed in winter, when the Agulhas Current is comparatively shallow and weak

Correspondence to:
L. Braby,
lv.braby@saeon.nrf.ac.za

Citation:
Braby, L., Deshayes, J., Beal, L., Morris, T., Novelli, G., Maitland, J., et al. (2022). First observations of seasonal variability in water mass properties across the Agulhas Current. *Journal of Geophysical Research: Oceans*, *127*, e2021JC018107. https://doi.org/10.1029/2021JC018107

Received 15 OCT 2021
Accepted 28 AUG 2022

© 2022. The Authors.
This is an open access article under the terms of the Creative Commons Attribution License, which permits use, distribution and reproduction in any medium, provided the original work is properly cited.

1. Introduction

The Agulhas Current forms the western limb of the South Indian Ocean subtropical gyre (Lutjeharms, 2006), carrying heat and salt away from the tropics and toward the poles as part of the global climate system (Beal et al., 2011). Several studies have investigated the seasonality of the Agulhas Current over the last decade. An altimetry-based study by Krug and Tournadre (2012) suggested that the flow is stronger during austral summer. This has been corroborated by the work of Beal et al. (2015) and Elipot and Beal (2015) who use three years of mooring observations from the Agulhas Current Time-series experiment (ACT, 2010 to 2013) to find a transport maximum during austral summer. Further work by Hutchinson et al. (2018) used an idealized model to suggest that the phasing of this observed seasonality is linked to a westward-propagating baroclinic adjustment to near-field wind forcing. Numerical ocean models to date have been unable to capture the observed seasonal phasing (Biastoch et al., 1999; Matano et al., 2002).

21699291, 2022, 9, Downloaded from https://agupubs.onlinelibrary.wiley.com/doi/10.1029/2021JC018107 by Cochrane France, Wiley Online Library on [12/10/2022]. See the Terms and Conditions (https://onlinelibrary.wiley.com/terms-and-conditions) on Wiley Online Library for rules of use; OA articles are governed by the applicable Creative Commons License

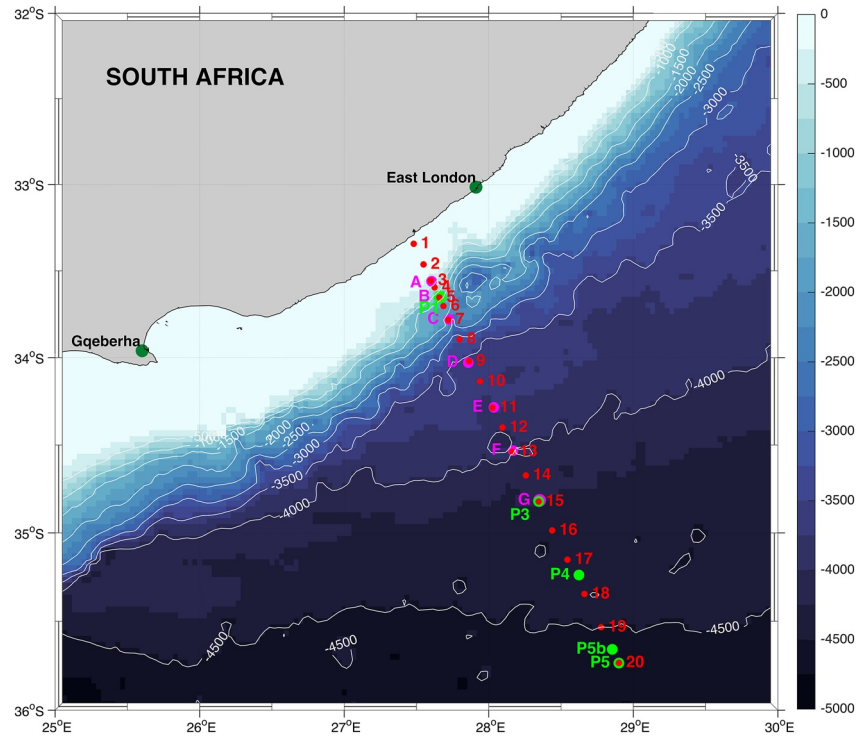

Figure 1. The approximate location of the Agulhas Current time-series experiment (ACT)/agulhas system climate array (ASCA) transect in relation to the South African coastline; shading indicates the bathymetry (m) with the geographical location of each CTD sampling station denoted by red dots. The magenta dots represent the positions of the full-depth ASCA moorings, whilst green dots indicate the position of the ASCA current and pressure-sensor equipped inverted echo-sounders.

The interior modes of water mass variability and stratification change across the Agulhas Current have recently been explored using 26-month of moored temperature and salinity data from the Agulhas System Climate Array (ASCA; McMonigal et al., 2020; Gunn et al., 2020). Seasonal signals close to the surface, comprising warm waters in summer and cooler waters in winter, are consistent with higher net radiation during the summer months. However, deeper in the water column the seasonality is reversed, with cooler thermocline and intermediate waters in summer. This is related to the upward tilt of density surfaces during the summer months when the current is stronger, consistent with geostrophic balance (McMonigal et al., 2020).

Here, we further characterize the seasonality of the Agulhas Current and its water masses using eight hydrographic cross-sections (with the four complete sections forming the bulk of our analysis) collected at the same location as the ACT and ASCA moorings (Figure 1) over the course of about a decade. Although these sections are very few compared to the daily sections from each of the mooring experiments, the ship-based data have far greater spatial detail than the point measurements from the moorings. Each hydrographic section consists of 20 CTD stations, compared to the nine mooring sites, and has an order of magnitude better vertical resolution than the point measurements from the moored instruments. The ASCA moorings resolve the velocity field and property transports of the entire Agulhas Current tolerably well, as per design (Gunn et al., 2020; McMonigal et al., 2020), but some water mass features in the upper water column are not captured by the moorings. This is because while velocities throughout the upper water column are measured remotely using upward-facing Doppler current profilers, temperature and salinity are measured only directly at the instrument positions (Figure 8, pink boxes). The moored instruments are subject to several hundred meters of blow down resulting in large sampling gaps over the upper water column. These gaps were exacerbated by instrument losses at moorings B and G during ASCA. McMonigal et al. (2020) approached this issue with some success by merging daily satellite Sea Surface Temperature (SST) data with the ASCA temperature observations. But for salinity, Gunn et al. (2020) found that the large footprint of satellite Sea Surface Salinity data could not capture the sharp cross-stream gradients of the Agulhas Current and hence the subsurface salinity maximum of subtropical surface waters was only intermittently resolved.

21699291, 2022, 9, Downloaded from https://agupubs.onlinelibrary.wiley.com/doi/10.1029/2021JC018107 by Cochrane France, Wiley Online Library on [12/10/2022]. See the Terms and Conditions (https://onlinelibrary.wiley.com/terms-and-conditions) on Wiley Online Library for rules of use; OA articles are governed by the applicable Creative Commons License

Table 1
CTD Surveys Across the Agulhas Current Along the Agulhas System Climate Array (ASCA) Line at 34°S

Experiment	CTD deployment dates	Seasonal classification	Agulhas Current state	CTD stations and depths	ADCP frequency and type
ACT	17–19 April 2010	Autumn	Meander	Stations 1–20, full depth	300 kHz S-ADCP, 300 kHz, L-ADCP
	20–23 November 2011	Summer	Non-meander	Stations 1–20, full depth	150 kHz S-ADCP, 300 kHz, L-ADCP
	14–15 February 2013	Summer	Non-meander	Stations 1–20, full depth	150 kHz S-ADCP, 300 kHz, L-ADCP
ASCA	20–21 April 2015	Autumn	Non-meander	Stations 1–16, to a maximum depth of 1,102 m only	150 kHz, S-ADCP
	7–11 July 2016	Winter	Non-meander	Stations 1–20, full depth	75 kHz, S-ADCP
	22 January 2018	Summer	Non-meander	Stations 1–7, to a maximum depth of 1,976 m only	150 kHz, 75 kHz, S-ADCP
	19–23 July 2018	Winter	Non-meander	Stations 1–20, full depth	75 kHz, S-ADCP
	3–8 July 2019	Winter	Non-meander	Stations 1–16, full depth except for stations 4–8	75 kHz, S-ADCP

In our analysis, we exploit the first austral winter cross-sections of the Agulhas Current, collected along the ASCA line as part of the South African SEAmester programme (https://seamester.co.za/). Two full crossings and one partial crossing were occupied by the SA Agulhas II during the winters of 2016, 2018, and 2019, each consisting of full-depth CTD casts and underway Acoustic Doppler Current Profiler (S-ADCP) measurements (Figure 1).

2. Data and Methods

2.1. Hydrographic Data

We gathered together all eight existing hydrographic sections across the Agulhas Current along the ASCA line close to 34°S (Figure 1). The ASCA line is 300 km long and crosses the Agulhas Current at an angle of about 15° south of cross-stream, following a satellite altimeter ground track that has been sampled for almost three decades (Figure 1; Beal & Elipot, 2016a, 2016b). Two mooring arrays have been deployed along the ASCA line, the ACT velocity array from 2010 to 2013 (Beal et al., 2015) and the ASCA velocity, temperature, and salinity array from 2016 to 2018 (McMonigal et al., 2020). During each hydrographic survey up to 20 CTD stations and continuous S-ADCP velocity measurements were collected.

2.1.1. CTD Data

The CTD sections all consist of the same 20 repeated stations, beginning with station 1 in less than 100 m of water over the shelf and ending with station 20 in more than 4,000 m of water at a distance of 300 km offshore (Figure 1). However, hydrographic winch capabilities, as well as weather and swell conditions sometimes limited operations and therefore only five out of the eight surveys are complete. Table 1 shows the dates and austral season of each survey, the station numbers occupied, and the maximum depth of the CTD casts.

The three complete surveys from 2010, 2011, and 2013 were collected as part of the ACT experiment and these data have been published previously (Leber & Beal, 2014, 2015; Leber et al., 2017). Here we carefully processed and calibrated the new CTD data from the three winter SEAmester surveys using Seabird software and following GO-SHIP best-practices. For the July 2016 survey, we observed higher salinity values from the samples collected from deeper water masses than previously recorded across the transect, we also found the range in salinity values from the salinometer to be too broad. For these reasons we opted to use the uncorrected, processed CTD data as the final salinity data for the July 2016 survey. In the case of the July 2018 surveys, salinity bottle samples were stored ashore for some months before they could be analyzed due to a malfunction of the salinometer. As a result, the accuracy of these data falls short of the international standard, with a final error of 0.0037 psu, although the salinities compare well with the ACT data. For the 2019 survey, salinity samples were run during the cruise and the internationally accepted standard was achieved, with a final error of 0.002 psu. The extended salinity processing reports show how these salinity data from the winter surveys compare with historical data collected across the transect (https://doi.org/10.5281/zenodo.6546449k).

21699291, 2022, 9, Downloaded from https://agupubs.onlinelibrary.wiley.com/doi/10.1029/2021JC018107 by Cochrane France, Wiley Online Library on [12/10/2022]. See the Terms and Conditions (https://onlinelibrary.wiley.com/terms-and-conditions) on Wiley Online Library for rules of use; OA articles are governed by the applicable Creative Commons License

Table 2
Water Masses of the Agulhas Current (Adapted From Beal et al., 2006)

Abbreviation	Water mass	Neutral density
TSW	Tropical surface water	<25.5
STSW	Subtropical surface water	25.5–26.4
SICW	South Indian central water	26.4–27.0
AAIW and RSW	Antarctic intermediate water and red sea water	27.0–27.92
NADW	Upper north atlantic deep water	27.92–28.08
NADW	Lower north atlantic deep water	>28.08

We define water masses according to their neutral densities (Table 2) following Beal et al. (2006). The North Atlantic Deep Water (NADW) is split into 2 layers, namely the Upper and Lower NADW, with the Lower NADW defined as the layer that is enclosed farther downstream by the regional topography of the Natal Valley (Beal et al., 2006).

2.1.2. ADCP Data

Shipboard ADCP data were collected continuously during all surveys (Table 1), resulting in both outbound and inbound velocity transects. For our purpose, we follow the preferred method described by Beal and Bryden. (1999) and estimate on-station velocity profiles by averaging all the S-ADCP data collected during the time of each CTD cast, typically on the outbound transect. During the 2010, 2011, and 2013 surveys ADCPs were also lowered with the CTD package, providing a measure of velocity throughout the water column, including accurate bottom-tracked velocities within about 100 m of the sea bed. These data were merged with the on-station S-ADCP profiles, using the LADCP inverse processing method from Visbeck (2002), to create full depth velocity profiles at each station along the transect (Leber & Beal, 2014). For the SEAmester surveys there are no L-ADCP data. A 75 kHz S-ADCP collected velocity profiles down to 650 m depth, on average.

2.1.3. Calculating Geostrophic Velocity and Estimating a Reference Velocity

To estimate geostrophic velocity from temperature and salinity measurements, we use the dynamic method:

$$v = \frac{1}{fL}(\Delta D_2 - \Delta D_1) + v_{\text{ref}} \tag{1}$$

where f is Coriolis force, L is the distance in km between CTD stations 1 and 2 and $\Delta D_1, \Delta D_2$ are the dynamic height anomalies at these stations. We estimate the unknown reference velocity, v_{ref} following the method described by Beal and Bryden. (1997, 1999). First, we interpolate our on-station ADCP velocity profiles onto station pairs to compare to the geostrophic velocity profiles (Figure 2). We then used the difference between the depth-averaged ADCP velocities $\overline{v}_{\text{ADCP}}$) and the depth-averaged geostrophic velocities ($\overline{v}_{\text{baroclinic}}$), over their common depths, to find a reference velocity.

$$v_{\text{ref}} = \overline{v}_{\text{ADCP}} - \overline{v}_{\text{baroclinic}} \tag{2}$$

Only velocities below 200 m were used in the calculation, as the ADCP velocities near the surface have a significant ageostrophic (Ekman) component due to the wind.

When available, the combination of S-ADCP and L-ADCP giving full-depth direct velocities yielded robust estimates of v_ref. For the winter occupations the 75 kHz S-ADCP was restricted to the upper 650 m depth, leaving most of the water column and bottom velocities unmeasured (Figure 2). The standard deviation of the averaged S-ADCP profiles collected at each station pair is large over the upper water column (in the region above 200 m) and results in errors of order 10 cm s^{-1} in the estimated geostrophic reference velocity. This uncertainty translates into spurious deep northward geostrophic velocities on the three station pairs shown in Figure 2.

21699291, 2022, 9, Downloaded from https://agupubs.onlinelibrary.wiley.com/doi/10.1029/2021JC018107 by Cochrane France, Wiley Online Library on [12/10/2022]. See the Terms and Conditions (https://onlinelibrary.wiley.com/terms-and-conditions) on Wiley Online Library for rules of use; OA articles are governed by the applicable Creative Commons License

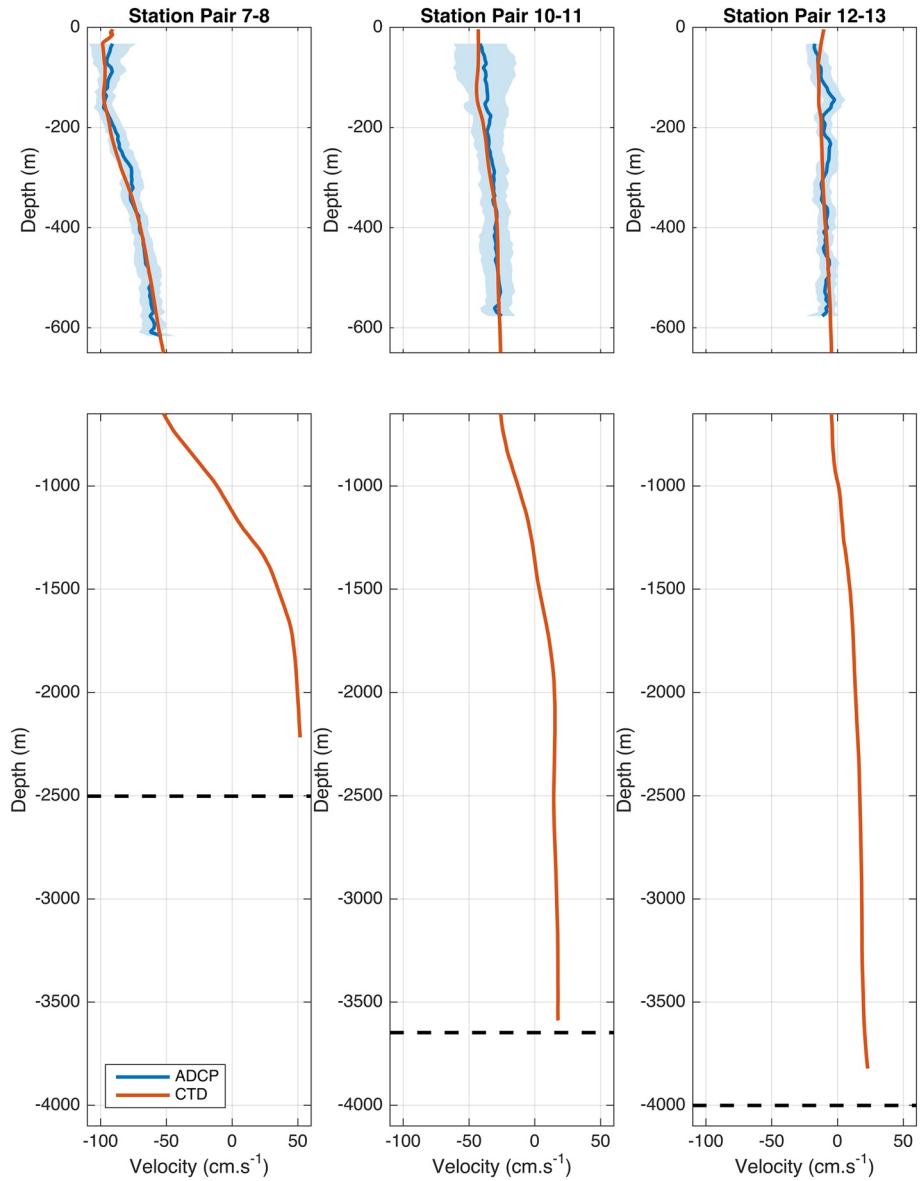

Figure 2. S-ADCP velocity (blue) and referenced geostrophic velocity (orange) from three station pairs during the July 2018 survey. Pale blue shading indicates the range of S-ADCP profiles that go into the average. Dashed black lines indicate the depth of the sea floor at the shallowest station of the pair.

2.2. Mooring Data

2.2.1. ACT Proxy Data

A time series of Agulhas Current proxy transports, with a 10 days temporal resolution, were used to determine the mean seasonal cycle of Agulhas Current boundary layer transport across the ACT/ASCA transect from 1993 to 2015. This data set combines 3 years of ACT mooring data with along-track altimeter data and is best described by Beal and Elipot (2016a, 2016b).

2.2.2. ASCA Mooring Data

The 26 months gridded ASCA mooring data were used to highlight strengths and shortcomings of the CTD data. The mooring temperature, salinity and velocity data provides much information about the seasonal cycle of the Agulhas Current which can be used to validate some of the seasonal features we observe in the hydrographic data.

21699291, 2022, 9, Downloaded from https://agupubs.onlinelibrary.wiley.com/doi/10.1029/2021JC018107 by Cochrane France, Wiley Online Library on [12/10/2022]. See the Terms and Conditions (https://onlinelibrary.wiley.com/terms-and-conditions) on Wiley Online Library for rules of use; OA articles are governed by the applicable Creative Commons License

21699291, 2022, 9, Downloaded from https://agupubs.onlinelibrary.wiley.com/doi/10.1029/2021JC018107 by Cochrane France, Wiley Online Library on [12/10/2022]. See the Terms and Conditions (https://onlinelibrary.wiley.com/terms-and-conditions) on Wiley Online Library for rules of use; OA articles are governed by the applicable Creative Commons License

Both the ACT proxy data and the ASCA mooring data are freely available online at https://beal-agulhas.rsmas.miami.edu/data-and-products/.

2.3. Satellite Observations

Satellite data give spatial context to the *in situ* measurements, providing information about the upstream and offshore conditions. We use daily MODIS-AQUA sea surface temperature (SST) data, a level 3 product with a resolution of 4 km (https://podaac.jpl.nasa.gov/), and daily, gridded maps of Absolute Dynamic Topography (ADT) at a resolution of 0.25° (https://marine.copernicus.eu/). Figure 3 shows the SST and ADT fields averaged over the 2–3 days it took to occupy each CTD section. The Agulhas Current is often covered by clouds and hence the non-blended level 3 SST product only supplies partial coverage. The cloud cover occurring above the Agulhas Current during the January 2018 survey was particularly problematic and therefore we included data from the day preceding and the day succeeding the survey in our averaged field (Figure 3f). In spite of these gaps, we found that the MODIS-AQUA product compared most closely with the CTD data collected along the ASCA transect compared to the level 4 SST products we investigated.

For the purposes of our investigation into seasonal signals we focus, for the most part, on the data from the four full surveys corresponding to summers 2011 and 2013 (Figures 3b and 3c), and winters 2016 and 2018 (Figures 3e and 3g). The survey in 2010 is anomalous, since it was conducted during a large meander of the Agulhas Current (Leber & Beal, 2014, Figure 3b). The survey in 2015 (Figure 3d) only covers the top 1,000 m (Table 1), and those in January 2018 and July 2019 (Figures 3f and 3h) have significant data gaps at the core of the current which, for the sake of our analysis into small differences between occupations, proved insurmountable. An offshore cyclone is present during the July 2018 survey. These eddies frequently occur in this region and we opt to keep this survey as a part of our seasonal analysis. We do, however, consider the possible impact that this eddy could have on the water mass distribution.

We linearly interpolated the four complete CTD datasets onto a regular spatial (x-z) grid, with bins corresponding to the mean distance and depths across all CTD surveys, as well as onto a neutral density (x-gamma) grid with bins of 0.01 $kg.m^{-3}$. We then calculate differences in both depth and density space.

3. Results

3.1. How Well Can the Few Available CTD Surveys Capture Seasonal Signals?

To develop confidence that we can estimate seasonal signals from the very few hydrographic surveys available we compared a daily climatology from a decade of MODIS-AQUA SST data along the ASCA line with the CTD surface temperature data (Figure 4). We define the MODIS summer mean as the average over months December, January, February, and the MODIS winter mean as the average over months June, July, August. Gaps in the SST data, resulting from cloud cover, were not included in the seasonal mean calculation. Any reasonable choice of seasonal averaging yields similar results. This robust seasonal climatology of SSTs was then compared to the near-surface seasonal temperature signals approximated from the sparse CTD data (Figure 4).

We define the CTD summer mean near-surface temperature as the average of the shallowest CTD data bins (9 m, except for a few stations where CTD data did not reach the surface) from the gridded 2011 and 2013 transects and similarly for the CTD winter mean from the gridded 2016 and 2018 transects. The November survey began just 10 days prior to the start of the austral summer season (typically defined as December, January, and February) and sea surface temperatures across the transect were notably cooler than the average satellite temperatures for summer (Figure 4a), although somewhat typical for the month of November (Figure 4b). The February survey, however, occurred right at the end of the summer season and is slightly warmer than the mean and standard deviation of the summer temperature demonstrated by the MODIS satellite data. Our 2 summer surveys thus occur at the beginning and end of the season.

The CTD and MODIS seasonal temperature signals are well matched, with a root mean square difference of 0.8°C in summer and 0.1°C in winter (Figure 4a). These discrepancies are much smaller than the seasonal signal. The largest discrepancies are found close to the coast in summer, where the CTD data are 4°C cooler than MODIS. This could be due to limitations of the satellite SST data near land or to low cloud coverage during summer upwelling events. Differences between SST skin temperature and *in situ* temperature at 9 m depth are not uncommon in summer, when strong insolation can build large vertical temperature gradients (Carr

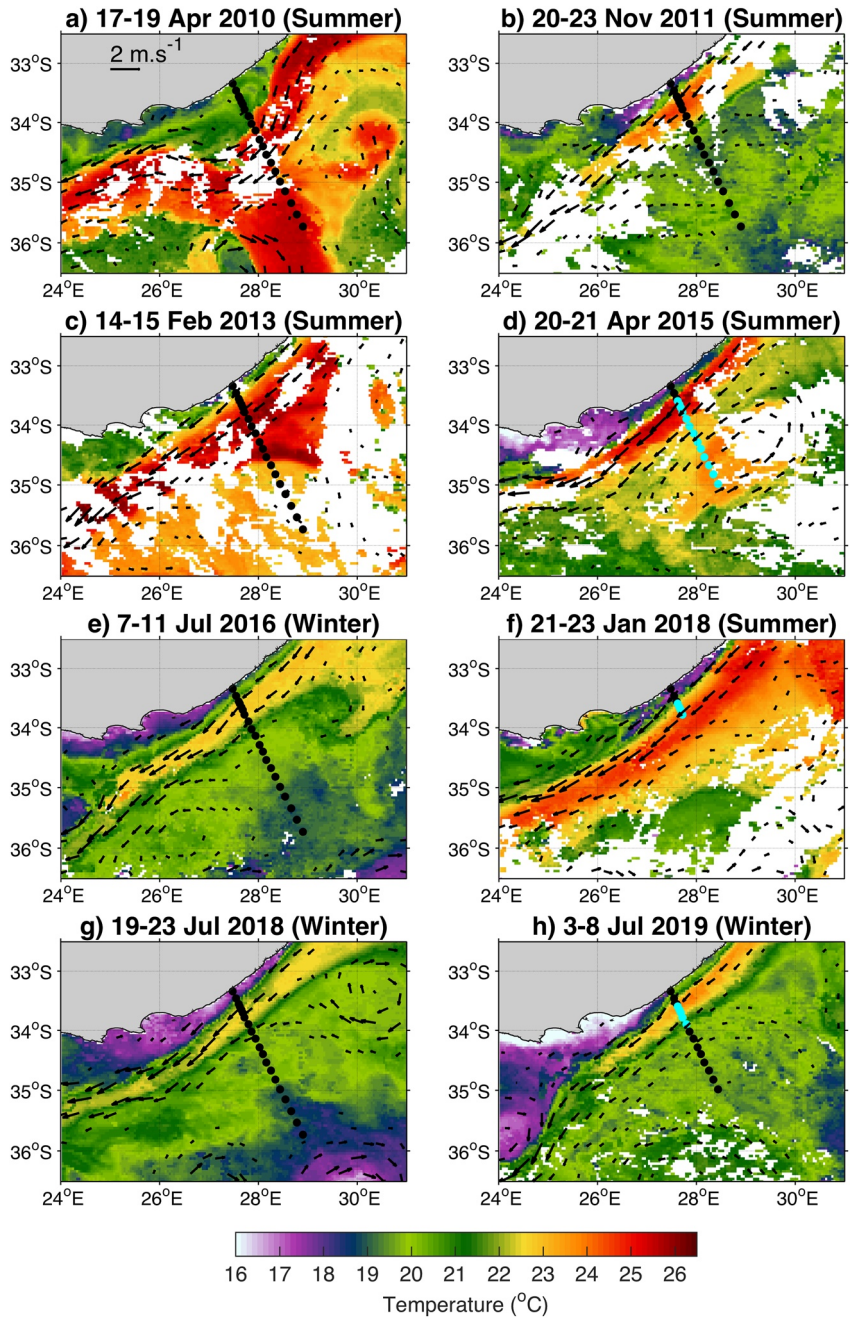

Figure 3. MODIS-AQUA sea surface temperature (°C) averaged over the CTD sampling period of the agulhas current time-series experiment/agulhas system climate array array cruises for (a) April 2010, (b) November 2011, (c) February 2013, (d) April 2015, (e) July 2016, (f) January 2018, (g) July 2018, and (h) July 2019. Black dots represent the positions of the full depth CTD stations, whilst light blue dots represent the non-full depth CTD stations occupied for each survey. Black vectors indicate direction of flow for geostrophic velocities greater than 0.3 $m.s^{-1}$. The figure labels indicate whether surveys are classified as summer or winter for the seasonal analysis in this study.

et al., 2021; Minnett et al., 2011). The large differences in surface temperature between the two summer CTD surveys are consistent with variance observed in the satellite data (Figures 3b and 3c). Leber and Beal. (2014) reason that cooler surface waters might be expected on the section occupied at the beginning of summer (November) in comparison to the one occupied in late summer (February). The MODIS data indicates that the mean SST is 1.38–3.8°C warmer across the transect in February compared to November (Figure 4b). Whilst we don't have enough hydrographic sections to focus on the differences between the beginning and end of the summer season,

21699291, 2022, 9, Downloaded from https://agupubs.onlinelibrary.wiley.com/doi/10.1029/2021JC018107 by Cochrane France, Wiley Online Library on [12/10/2022]. See the Terms and Conditions (https://onlinelibrary.wiley.com/terms-and-conditions) on Wiley Online Library for rules of use; OA articles are governed by the applicable Creative Commons License

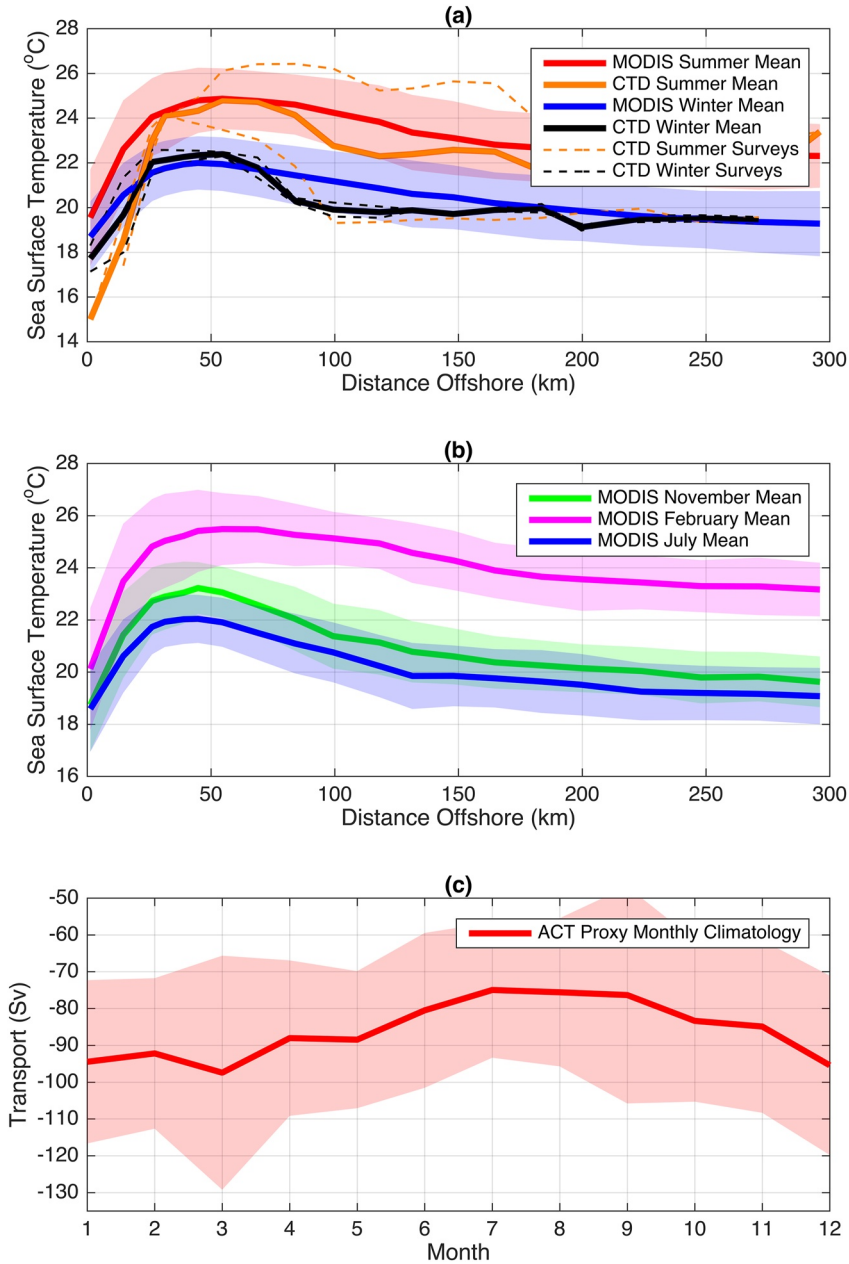

Figure 4. (a) Sea surface temperature (SST) summer and winter means across the Agulhas Current time-series experiment (ACT)/agulhas system climate array transect from 2010 to 2019. Mean surface CTD temperatures are indicated in orange for non-meandering summer occupations of the Agulhas Current, and black during the winter occupations. Satellite SST means are indicated in red during summer and blue during winter. The red and blue shading denote seasonal satellite standard deviations from 2010 to 2019 across the transect for summer and winter, respectively. Orange (black) dashed lines demonstrate the SST for the individual summer (winter) CTD surveys of the transect, (b) monthly means and standard deviations of satellite SST that correspond to the months of the summer and winter sections with November shown in green, February in magenta and July in blue and (c) the monthly climatology and standard deviation of Agulhas Current boundary layer transport from the ACT proxy data.

our 1 time data (Figure 4a) represents the seasonal warming which can be expected over the summer season. The November SST's are on average 0.15–1.18°C warmer than July temperatures. The variances in the hydrographic winter SSTs are much smaller than those observed in the summer surveys.

Whilst sea surface temperatures are notably different between the November and February surveys, there are other similarities throughout the rest of the water column. The upwelling of central waters onto the continental

21699291, 2022, 9, Downloaded from https://agupubs.onlinelibrary.wiley.com/doi/10.1029/2021JC018107 by Cochrane France, Wiley Online Library on [12/10/2022]. See the Terms and Conditions (https://onlinelibrary.wiley.com/terms-and-conditions) on Wiley Online Library for rules of use; OA articles are governed by the applicable Creative Commons License

21699291, 2022, 9, Downloaded from https://agupubs.onlinelibrary.wiley.com/doi/10.1029/2021JC018107 by Cochrane France, Wiley Online Library on [12/10/2022]. See the Terms and Conditions (https://onlinelibrary.wiley.com/terms-and-conditions) on Wiley Online Library for rules of use; OA articles are governed by the applicable Creative Commons License

shelf observed in the summer surveys is also evident in the November occupation of the current (Figure 8). Additionally, the cooler, fresher waters observed below the mixed layer depth during summer are evident in both the November and February surveys. Removing the November data from the summer mean yields a similar result for Figure 9. We therefore opt to categorize the November survey as a summer survey of the current.

Turning to seasonal differences in surface temperature, we find that both the CTD and MODIS data show that the inshore temperature front of the Agulhas Current is stronger in summer than in winter, although the signal is far smaller in the MODIS climatology. The temperature difference between the core of the Agulhas Current and the shelf waters from the *in situ* data is 8 and 10°C in summer (4.3°C from MODIS) and 5–6°C in winter (3.8°C from MODIS). The stronger temperature gradients observed in summer are consistent with the occurrence of more upwelling-favorable winds at that time of year, which cause cool central waters to outcrop over the shelf (Leber et al., 2017; Lutjeharms, 2006; Lutjeharms et al., 2000; Schumann, 1982). The upwelling-favorable wind observed during the February 2013 cruise (Leber et al., 2017) may contribute to some of the differences observed between climatological SST and the CTD mean.

Our comparison of the MODIS seasonal climatology with the averaged summer and winter in situ occupations (Figure 4) gives us confidence that we can attribute water mass differences between these few summer and winter occupations as indicative of seasonal variability. This paper focuses on seasonal differences across the ACT/ASCA transect which are observed deeper in the water column. A monthly climatology of Agulhas Current boundary layer transport from the ACT proxy data (Figure 4c) show the seasonal variation of Agulhas Current transport, with stronger net transports exceeding −90 Sv during the summer season, relative to net transports of between −74.98 and −80.50 Sv during the winter months. Below the thermocline, we expect differences observed are largely due to changes in the strength of the Agulhas Current.

3.2. Cross-Sections of the Agulhas Current in Winter and Summer

From the SEAmester cruises we have the first full-depth hydrographic cross-sections of the Agulhas Current along the ASCA line occupied in winter (Figure 5). There are deep reversals in geostrophic velocity on three or four station pairs of the winter 2018 occupation (Figure 5b). These appear unrealistic given the lack of correlation in the flow from one station pair to the next and what we know about the correlation length scales of deep velocities from the moorings (Beal et al., 2015). We put these features down to uncertainties in the reference velocities estimated from the S-ADCP (Figure 2).

The current is stronger and narrower in winter 2018 than in winter 2016 because the leading edge of a cyclonic anomaly lifts the isopycnals at the offshore flank of the jet during the 2018 transect (Figures 3g and Figure 5b). The upper 200 m of the water column are most affected, with tropical surface waters (gamma <25.5) confined to within 200 km of the coast.

Comparing the summer occupations (Figure 6) with the winter occupations (Figure 5), we find no significant difference in the position or width of the current. However, we do find evidence for seasonality in the volume transport of the Agulhas Current. We calculate net transports of -94.5 ± 7.4 Sv for summer occupations of the transect, and net transports of -43.4 ± 4.3 Sv in winter (uncertainty in net transports is estimated here as the standard deviation in between different occupations for a given season). These differences in transport are presumably due to the Agulhas Current being stronger in summer (Beal and Elipot, 2016a, 2016b; Beal et al., 2015), although transport anomalies of water masses occurring along the ACT/ASCA transect are likely to contribute as well (see Figure 11 below) as we consider here the overall net transport through the whole section, full depth.

3.3. Seasonal Changes in Density Structure

To explore seasonal changes in the distribution and transport of each water mass within the Agulhas Current we created masks following the neutral density classifications of Beal et al. (2006) (Table 2) and applied them to all the available ASCA transects, save the anomalous meander section of 2010 (Figure 7). All the transects classified as summer are shown in the left column of Figure 7 and all the winter transects in the right column. The most notable difference between the seasons is the summer upwelling of central waters onto the shelf. This upwelling is persistent across all the summer transects except the one in April 2015 which is more accurately classified as an austral autumn occupation (Figure 7c). These data suggest that central waters are typically found in the lower water column of the inner shelf during summer and not during winter. Because the central waters do not outcrop at the surface, this *cryptic* upwelling is not visible by satellite and therefore largely unobserved. One implication

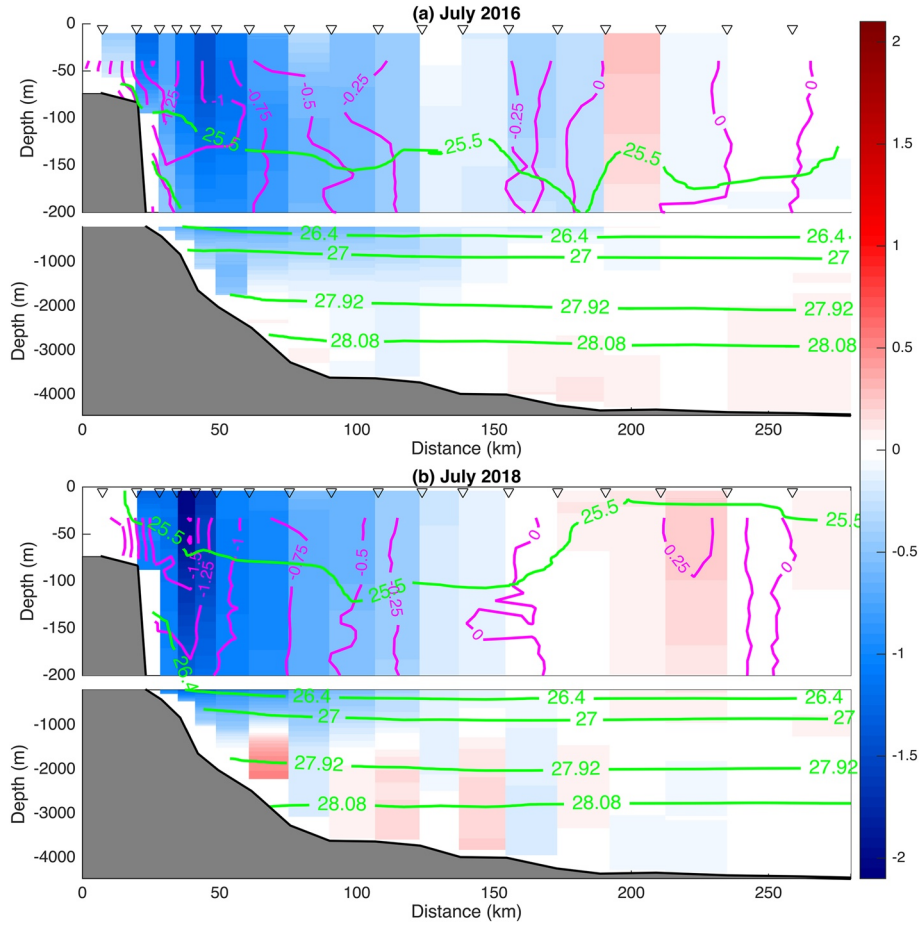

Figure 5. Winter velocity sections along the agulhas system climate array transect from (a) 2016 and (b) 2018 surveys. The shading in the upper panels show geostrophic velocities calculated from the CTD data, with on-station S-ADCP velocities rotated to their cross-track component overlaid in magenta contours. The lower panel shows geostrophic velocities referenced to the S-ADCP data, as explained in the Methods. Blue shades are poleward flow with the Agulhas Current, while red shades are equatorward flow. Green contours are neutral density surfaces that separate water masses (see Table 2). Dark gray shading is bathymetry and light gray shading are regions with no data. Black triangles mark the mean position of the station pairs used to calculate geostrophic velocity on each survey.

of this seasonal upwelling signal is that, in the depth-average, the waters over the shelf at this latitude are cooler during summer than winter, despite the stronger summer insolation.

The injection of cold, oxygen and nutrient-rich central waters onto the inner shelf during summer will have ramifications for productivity, recruitment, and ecosystems in these shallow, euphotic waters (Barlow et al., 2010, 2013; Beckley and van Ballegooyen, 1992; Lamont et al., 2018). A slight upwelling of the RSW/AAIW at the shelf is also observed during the summer occupations of the current but not during winter. A comparison of these observations with the neutral density determined from the gridded ASCA mooring data reveals several similarities and differences (Figure 8). The upwelling of SICW onto the shelf during the summer season is not observed in the mooring data. However, this is likely due to a lack of microcat instruments over the upper water column and self region (the region denoted by hatching). We do however observe an upwelling of RSW/AAIW water masses during summer in the mooring data, consistent with the CTD observations.

The upwelling of these central and intermediate water masses on the summer sections owes to the broad upward-tilt of the isopycnals across the Agulhas Current, which supports stronger poleward transport during summer (McMonigal et al., 2020). Local easterly and north-easterly winds can occur in the summer months and these may also play a role (Hutchings, 1994; Lutjeharms, 2006). The amount of upwelling is probably dependent on latitude and cross-shelf distance because of the role of topography, which can lift and fan out waters from

21699291, 2022, 9, Downloaded from https://agupubs.onlinelibrary.wiley.com/doi/10.1029/2021JC018107 by Cochrane France, Wiley Online Library on [12/10/2022]. See the Terms and Conditions (https://onlinelibrary.wiley.com/terms-and-conditions) on Wiley Online Library for rules of use; OA articles are governed by the applicable Creative Commons License

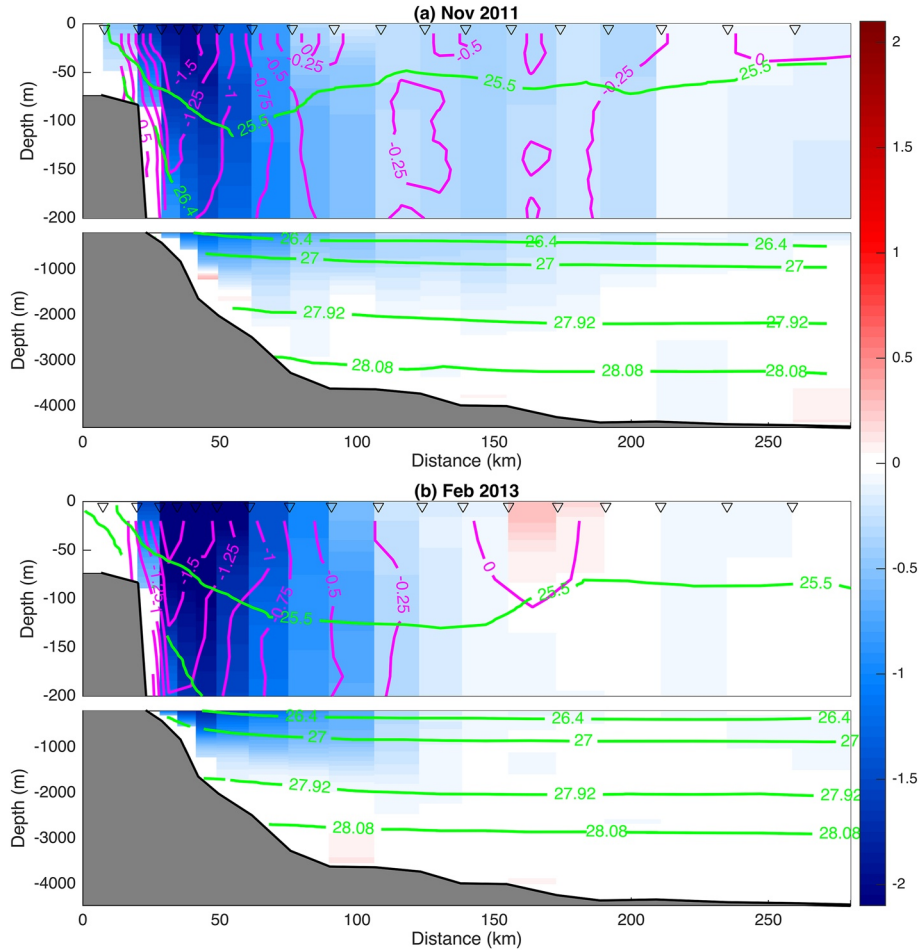

Figure 6. Velocities across the agulhas system climate array transect from (a) summer 2011, and (b) summer 2013 surveys. The shading in the upper 200 m of the water column shows geostrophic velocities calculated from the CTD data, with merged S-ADCP, L-ADCP velocities overlaid in magenta contours. Below 200 m, geostrophic velocities calculated from CTD data using the merged ADCP velocities as a reference are shown. Blue color indicates poleward flow, whereas red indicates equatorward flow. Green contours show lines of neutral density, denoting the different water masses present. Dark gray shading indicates the bathymetry and light gray shading indicates regions with no data. Black triangles mark the mean position of the station pairs used to calculate geostrophic velocity on each survey.

different depths (Gill & Schumann, 1979; Lutjeharms et al., 2000; Yang et al., 2018). This means that the strength and persistence of upwelling could be very different at another latitude.

3.4. Quantifying Seasonal Differences in Terms of Heave and Spice

To further investigate the processes behind seasonal water mass variability we calculate the difference between potential temperature and salinity in summer and winter in both depth- and density-space (Figure 9). Differences in depth-space illustrate dynamical changes due to the vertical displacement of density surfaces, while differences in density space illustrate changes in water mass properties along density surfaces.

As could be expected, surface waters are warmer and lighter during austral summer when there is net surface heating, with the largest differences in potential temperatures exceeding 4°C warmer at the surface than during winter (Figure 9a). This is consistent with seasonal temperature differences observed by McMonigal et al. (2020). Surface waters are also fresher during austral summer as a result of higher regional rainfall (Lutjeharms et al., 2000; Russo et al., 2019; Schumann, 1988, 1999). These surface-flux-driven signals, however, are constrained to depths of less than 100 m. This depth corresponds to the mean summer mixed layer depth, which we determined according to the method described by de Boyer Montégut et al. (2004). Below, cooler waters are evident throughout the

21699291, 2022, 9, Downloaded from https://agupubs.onlinelibrary.wiley.com/doi/10.1029/2021JC018107 by Cochrane France, Wiley Online Library on [12/10/2022]. See the Terms and Conditions (https://onlinelibrary.wiley.com/terms-and-conditions) on Wiley Online Library for rules of use; OA articles are governed by the applicable Creative Commons License

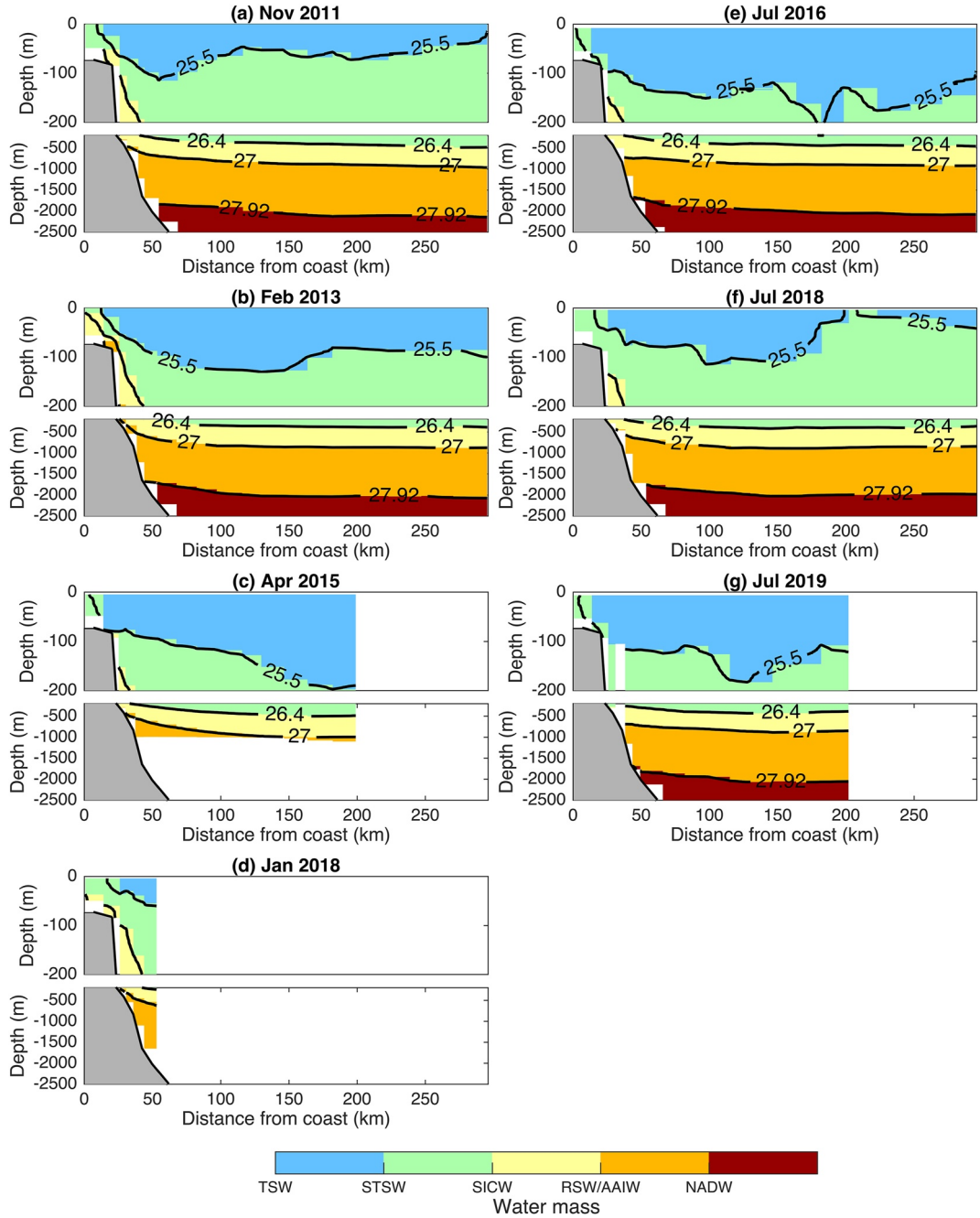

Figure 7. Distribution of the different water masses found in the upper 2,500 m on each agulhas system climate array transect. Black contours indicate lines of neutral density which separate each water mass. Blue shading indicates TSW, green the STSW, yellow the SICW, orange the AAIW and RSW, and red shading is NADW. Each sub-figure has two panels, with the upper panel focusing on the upper 200 m of the water column and the lower panel focusing on depths of 200–2,500 m.

subsurface water column (Figure 9a) and are driven by the tilting of density surfaces across the current during summer (Gunn et al., 2020; McMonigal et al., 2020). This broad-scale tilting also causes some warming on the offshore flank of the current. The seasonal difference in salinity has the same pattern as temperature, consistent with the upward tilt of density surfaces in summer (Figure 9b). This pattern supports the stronger geostrophic transport during summer (Beal and Elipot, 2016a, 2016b), which appears to be driven by near-field wind curl (Hutchinson et al., 2018).

21699291, 2022, 9, Downloaded from https://agupubs.onlinelibrary.wiley.com/doi/10.1029/2021JC018107 by Cochrane France, Wiley Online Library on [12/10/2022]. See the Terms and Conditions (https://onlinelibrary.wiley.com/terms-and-conditions) on Wiley Online Library for rules of use; OA articles are governed by the applicable Creative Commons License

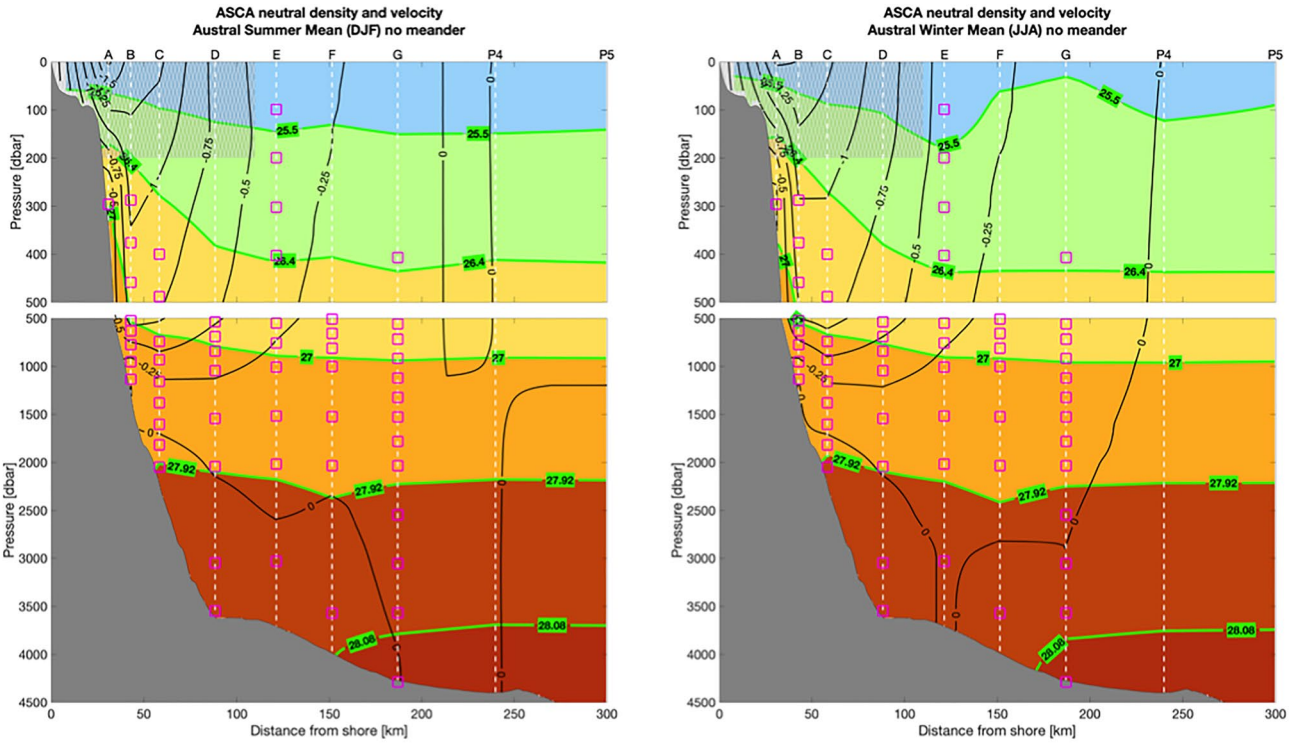

Figure 8. Neutral density (green contours) and water masses (shading as Figure 7) overlayed with velocity (black contours) from the mapped agulhas system climate array mooring data (McMonigal et al., 2020) for (a) Summer, averaged DJF and (b) Winter, averaged JJA. Pink boxes show the record median positions of instruments measuring temperature and salinity. Hatching over the upper, inshore water column highlights a region where mapped neutral density is highly uncertain because there are no moored T, S measurements. Here T and S are interpolated using contemporaneous satellite data and static vertical property gradients from historic hydrography (Details in McMonigal et al., 2020; Gunn et al., 2020). The historic hydrography was collected during summer and does not resolve seasonal changes.

It should be noted that the ASCA mooring data has a much lower spatial resolution than the hydrographic data used in this study. The mooring velocity data demonstrates the seasonal cycle of the Agulhas Current well (Figure 8) but does not capture the seasonal thermocline and seasonal upwelling over the slope that we find in our analysis of the CTD data. Since we know that the Agulhas Current is stronger during summer (observed in the mooring data, Figure 8), the isopycnals should slope in the mooring data in summer, even if this is only observed in the hydrographic data.

Two small-scale regions of strong cooling stand out on top of the broad cool/warm pattern (Figure 7). A thin ribbon of cool waters around 150 m depth could plausibly relate to subduction of warm Tropical Surface waters at the bottom of the winter-time mixed layer. This signal is not related to the anomalous uplift of density surfaces by the offshore cyclone in winter 2018, as disregarding this section yields a very similar result (not shown). Cool waters in the upper 500 m near the continental slope are the signature of dramatic upwelling of central waters over the topography, as seen previously in Figure 7. The counterintuitive result that shelf waters are cooler during summer was also observed by Russo et al. (2019).

By calculating the summer-winter property differences in density-space we eliminate the effect of heave, which otherwise dominates the seasonal signals (Figures 9c and 9d), to find the property differences due to spice anomalies. This means that the neutral density differences show differences with respect to isopycnals, rather than differences related to the movement of the isopycnals (Leber & Beal, 2015). Overall, seasonal signals in neutral density space are observed to be weaker than those in depth space. These differences relate to water mass changes either as a result of adiabatic processes, such as surface fluxes and mixing, or due to advection. We find cool, fresh spice anomalies at the base of the winter-time mixed layer related to subduction, as well as over the steep topography related to the upwelling of central waters. Since the mixed layer depth is deeper during winter than during summer, we expect the warm surface waters to extend deeper during the winter season, its signal still

21699291, 2022, 9, Downloaded from https://agupubs.onlinelibrary.wiley.com/doi/10.1029/2021JC018107 by Cochrane France, Wiley Online Library on [12/10/2022]. See the Terms and Conditions (https://onlinelibrary.wiley.com/terms-and-conditions) on Wiley Online Library for rules of use; OA articles are governed by the applicable Creative Commons License

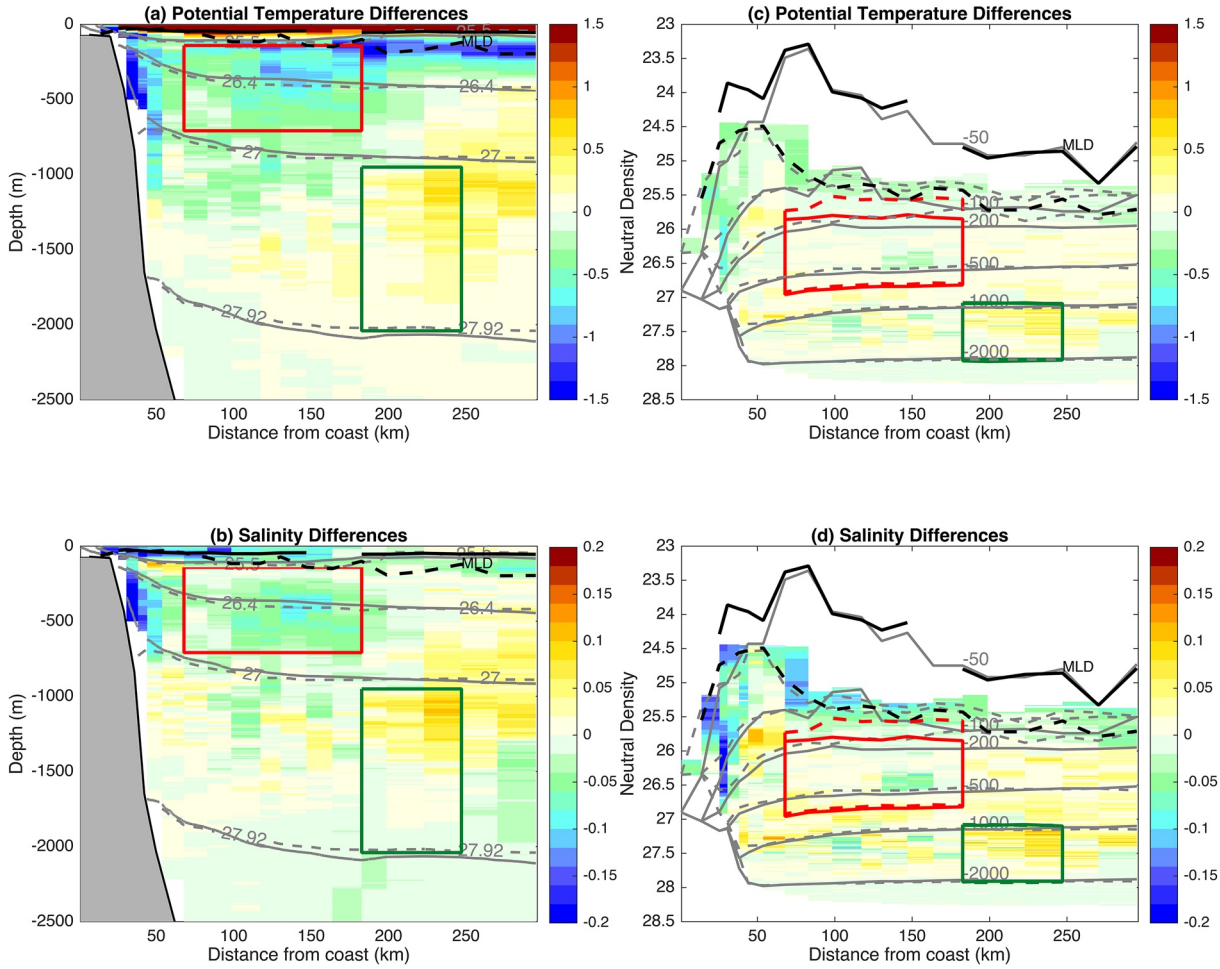

Figure 9. The difference between the mean summer and winter (a) potential temperature and (b) salinities across the agulhas current time-series experiment/agulhas system climate array transect, shown in depth space. Neutral density contours for summer (solid) and winter (dashed) are overlain in light gray. The difference between the mean summer and winter (c) potential temperature and (d) mean salinity represented in Neutral Density space. Gray contours indicate the mean depth during summer (solid) and winter (dashed). The mixed layer depth is shown with a black contour for summer (solid) and winter (dashed). The red and green boxes denote 2 regions with apparent seasonal differences from panels a and b of this figure.

being visible in neutral density space indicating that this difference is likely not caused by the seasonal changes in the strength of the Agulhas Current. The differences at the shelf imply that a large component of the upwelling of central waters is irreversible and acts to cool and freshen waters along the inshore front of the Agulhas Current. Throughout most of the rest of the water column there are warmer temperatures and higher salinities in summer and we are uncertain how to interpret these signals.

To further investigate the seasonal changes in water mass properties we define the red and green boxes on Figure 9 as regions with the largest seasonal differences that are remote from surface fluxes and topographic effects and plot their properties in a T/S diagram (Figure 10). The red box encompasses a region of negative summertime anomalies (cooler and fresher in summer), while the green box encompasses a region of positive anomalies. The negative anomalies all but disappear in neutral density space (Figures 9c and 9d), and indeed, in T/S space the difference between these water masses in summer and winter is small. This affirms that differences within the red box result from the summer tilt of the isopycnals. This is not the case, however, for the green box. The positive anomalies remain in neutral density space (Figures 9c and 9d) and are also visible in the T/S diagram (Figure 10), suggesting that at intermediate depths there may be a higher ratio of warm, salty RSW during summer (Figure 10).

21699291, 2022, 9, Downloaded from https://agupubs.onlinelibrary.wiley.com/doi/10.1029/2021JC018107 by Cochrane France, Wiley Online Library on [12/10/2022]. See the Terms and Conditions (https://onlinelibrary.wiley.com/terms-and-conditions) on Wiley Online Library for rules of use; OA articles are governed by the applicable Creative Commons License

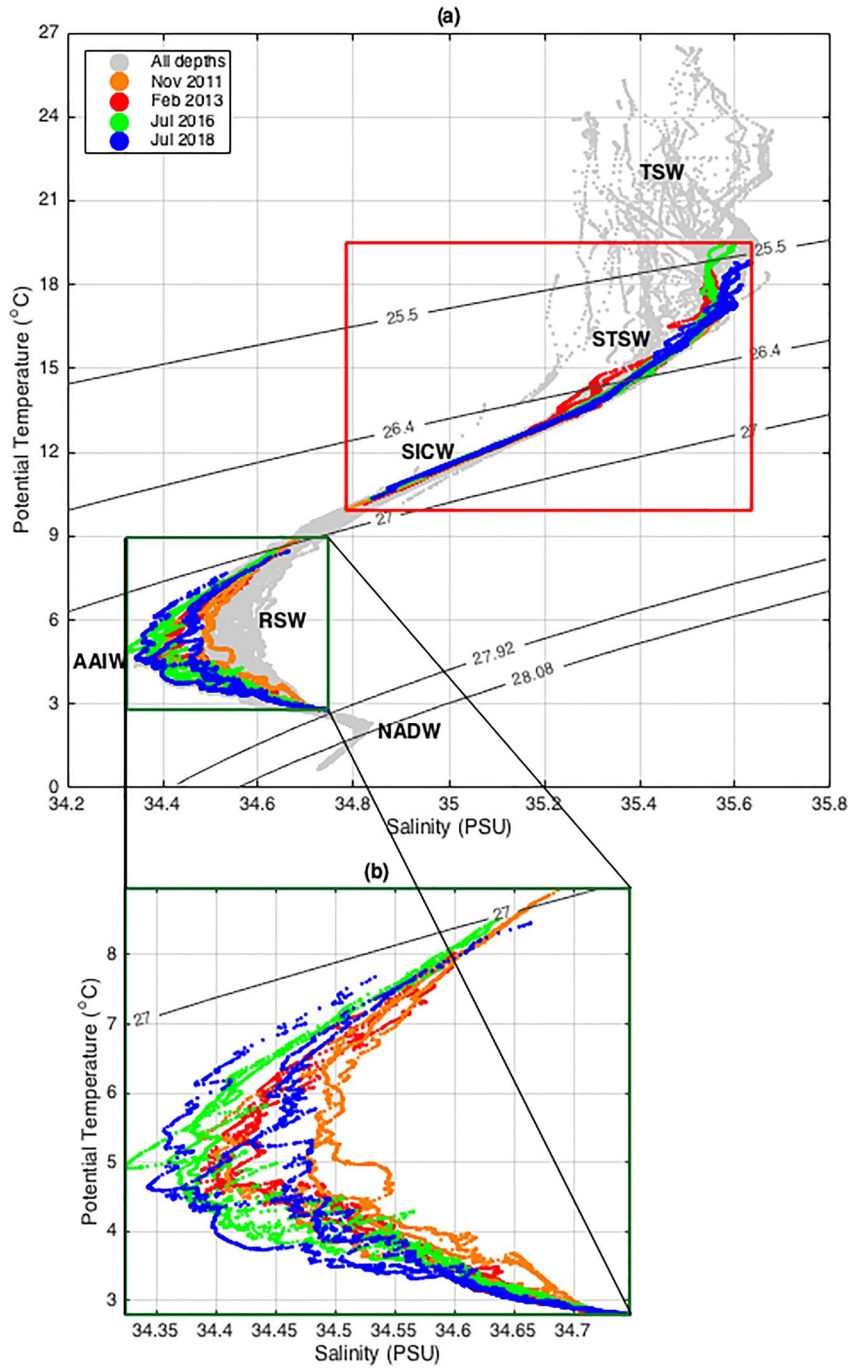

Figure 10. Potential temperature and Salinity values for all data points (gray) with (a) the red subset overlaid in color and (b) a close up of the green subset indicated previously. Colors correspond to the years indicated in the legend, with summer occupations in orange and red, while winter occupations are plotted in green and blue. Contours indicate the neutral density surfaces depicting the different water masses present.

3.5. Implications for Water Mass Transport Across the Section

All water masses have a stronger transport during summer than winter (Figure 11). We estimate the transport of each individual water mass by integrating the geostrophic velocities (Figures 5 and 6) within each water mass layer for each of the four complete sections (Figure 7). The transport in each layer is accumulated all the way along the section, from the coast to the farthest station offshore. The thickness of different water mass layers

21699291, 2022, 9, Downloaded from https://agupubs.onlinelibrary.wiley.com/doi/10.1029/2021JC018107 by Cochrane France, Wiley Online Library on [12/10/2022]. See the Terms and Conditions (https://onlinelibrary.wiley.com/terms-and-conditions) on Wiley Online Library for rules of use; OA articles are governed by the applicable Creative Commons License

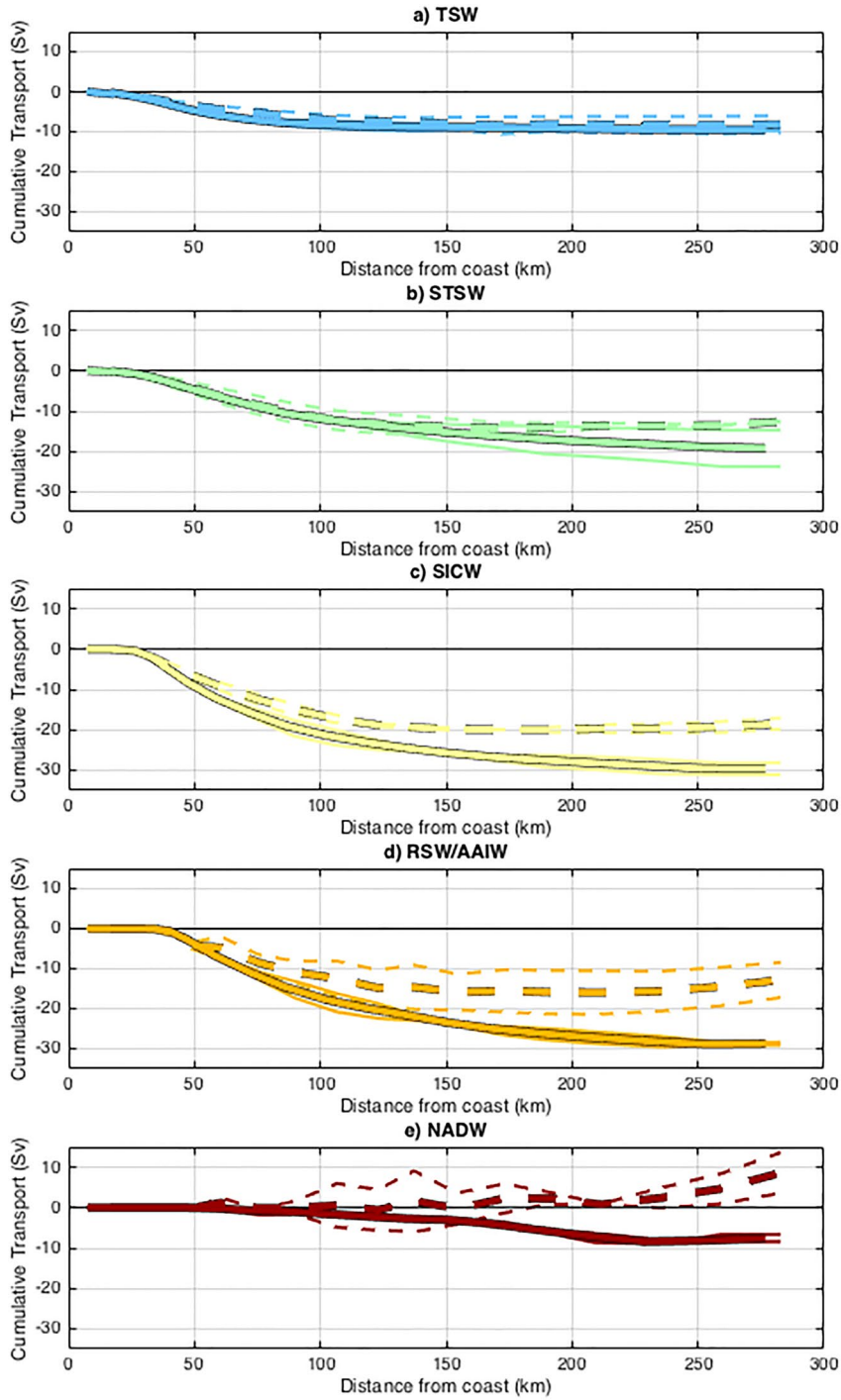

Figure 11. The mean summer and winter cumulative water mass transport across the agulhas system climate array transect for (a) TSW, (b) STSW, (c) SICW, (d) RSW/AAIW, and (e) NADW. Each water mass is represented by a different color (consistent with previous figures), where negative transports represent poleward flow and positive transports represent equatorward flow (see text for uncertainties in transport estimates). Bold solid lines represent summer transports and bold thick dashed lines are indicative of winter transports. Thin solid (dashed) lines show cumulative transports of the different water masses for individual summer (winter) surveys.

21699291, 2022, 9, Downloaded from https://agupubs.onlinelibrary.wiley.com/doi/10.1029/2021JC018107 by Cochrane France, Wiley Online Library on [12/10/2022]. See the Terms and Conditions (https://onlinelibrary.wiley.com/terms-and-conditions) on Wiley Online Library for rules of use; OA articles are governed by the applicable Creative Commons License

21699291, 2022, 9, Downloaded from https://agupubs.onlinelibrary.wiley.com/doi/10.1029/2021JC018107 by Cochrane France, Wiley Online Library on [12/10/2022]. See the Terms and Conditions (https://onlinelibrary.wiley.com/terms-and-conditions) on Wiley Online Library for rules of use; OA articles are governed by the applicable Creative Commons License

varies among the shallower water masses between different surveys but is fairly consistent among the deeper water masses. Despite this, the central, intermediate, and deep waters exhibit the largest differences between summer and winter transports. The direction of flow of NADW appears to switch, with net poleward transport in the direction of the Agulhas Current in summer and net equatorward transport in winter (Figure 11e). This seasonality is consistent in the context of the deepening and cooling of the current in summer when the transport is strongest, as observed in the mooring data (McMonigal et al., 2020). In this instance, however, the limitations of the geostrophic velocities calculated from the hydrographic data should be considered. Large errors in velocity are likely to occur at depth, and in some instances appear unrealistic (Figure 2). Some of this error could be attributed to a lack of L-ADCP measurements, with which to reference the calculated velocities. A comparison with the ASCA mooring data reveals equatorward and poleward flow of NADW across the transect during both the summer and winter seasons (Figure 8). Some seasonality of the NADW is observed, with equatorward flow observed across the majority of the transect during winter. At these depths, the mooring velocities are likely more robust than those determined from the hydrographic data.

The central and intermediate water masses contribute the largest volume of water to the total flow in each season, with a poleward SICW transport of 29.62 ± 2.08 Sv during summer and 18.44 ± 1.94 Sv during winter (Figure 11c), and a poleward RSW/AAIW transport of 28.71 ± 0.51 Sv during summer and 12.80 ± 6.19 Sv during winter (Figure 11d). The large differences between summer and winter may be partially due to the presence of mesoscale features in the vicinity of the transect (most visible in winter 2018, Figure 3g). Despite our reservations regarding the accuracy of the geostrophic velocities calculated from the hydrographic data at depth, the total net transports for both the summer and winter occupations across the ACT/ASCA transect (shown in Section 3.2) are comparable with estimates given by previous studies. These studies determine mean boundary layer transports and errors of −77 ± 5 Sv with a standard deviation of 32 Sv (Beal et al., 2015), and −75 ± 4 Sv with a standard deviation 26 Sv (McMonigal et al., 2020) from the ACT and ASCA mooring datasets, respectively.

4. Conclusion

We infer seasonal differences in water mass properties and transports within the Agulhas Current for the first time using 8 full-depth hydrographic sections. These sections are able to capture features in the upper water column and over the continental shelf that are unresolved by the Agulhas mooring array (ASCA).

Most significantly, we observe upwelling of central waters onto the continental shelf during summer occupations but not during winter. This upwelling is cryptic, meaning that the central waters do not outcrop at the surface and therefore are not visible from space. As a result, waters over the shelf are cooler and fresher, in the depth-average, during summer, despite higher summer insolation. We find that the summer upwelling of central waters is related to both an upward tilt in density surfaces across the Agulhas Current and to adiabatic effects over the continental slope. The tilting of density surfaces is consistent with larger geostrophic transport in summer and is thought to be driven by near-field wind stress curl (Hutchinson et al., 2018; McMonigal et al., 2020). Northeasterly winds in summer and offshore movement of the Agulhas jet also play a role in upwelling along the inshore edge of the Agulhas Current. These events can cause intermittent outcropping of the central waters that are visible via satellite (Leber et al., 2017; Lutjeharms et al., 2000).

Across the current and below the mixed layer waters are cooler during summer. This broad cooling pattern is due to the upward tilt of the density surfaces, which also drives some warming offshore. At intermediate depths, however, some of the offshore warming can be attributed to positive spice anomalies, suggesting that the ratio of RSW:AAIW along the section is greater during summer. We interpret this as linked to stronger recirculation of AAIW from more southerly latitudes in winter (Figure 12). Yet, since lenses and filaments of RSW are common (e.g., Gründlingh, 1985) and we have very few sections from which to infer seasonality, this signal may be aliased.

Below 2,000 m, we find that NADW flows equatorward across the section during winter, but is swept poleward with the stronger and deeper Agulhas Current in summer (Figure 12). McMonigal et al. (2020) found some seasonality of the NADW using the e ASCA mooring data. They found that deepening of the Agulhas Current into the NADW layer actually leads to cooler transport-weighted temperatures in summer. Since the geostrophic velocity sections calculated from the hydrographic data are so few, and some of the velocities at depth appear unrealistic (Figure 2) (perhaps due to a lack of L-ADCP measurements to reference these velocities), we caution to draw strong conclusions from the hydrographic data in this instance. We know however that the ASCA moor-

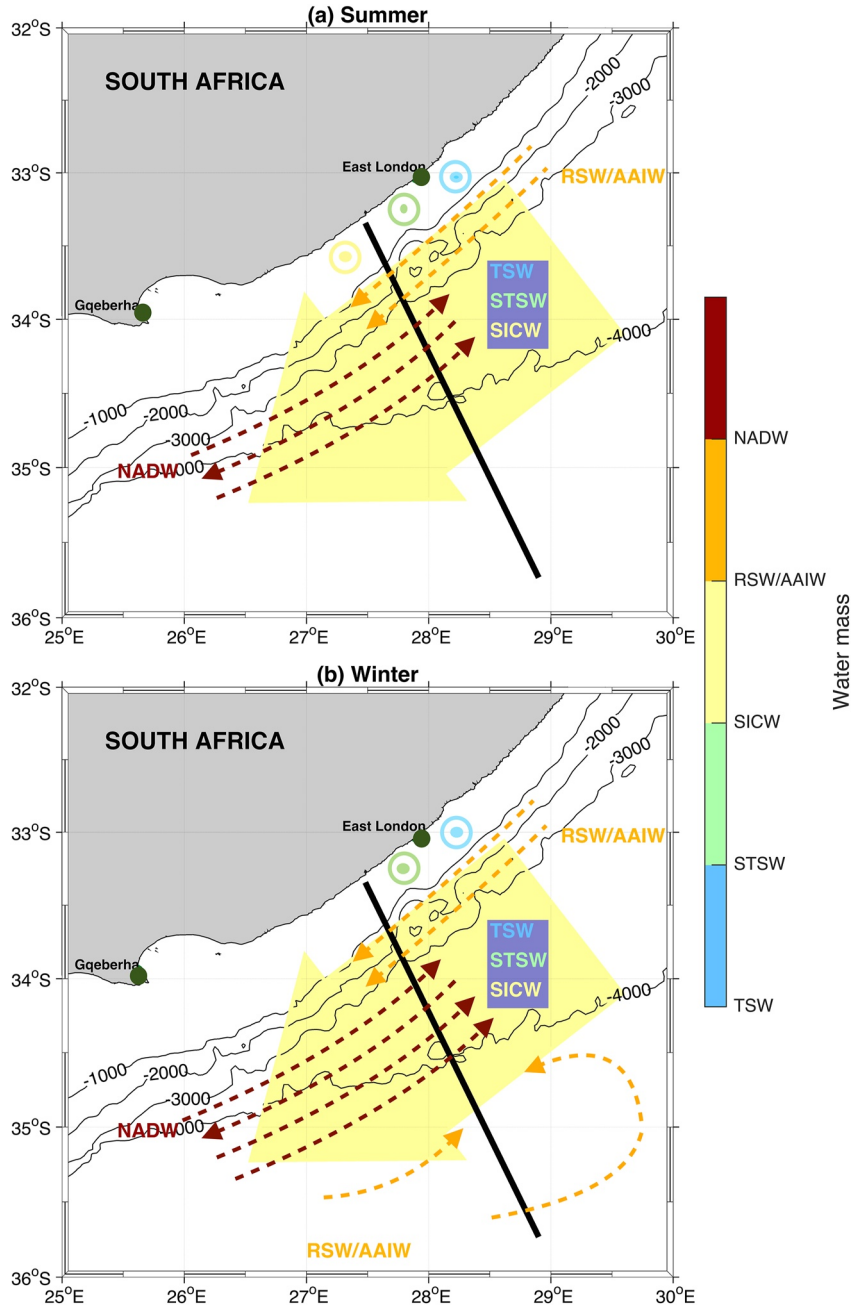

Figure 12. A schematic of water mass pathways across the agulhas current time-series experiment/agulhas system climate array transect (thick black line) based on hydrography measured during (a) summer 2011 and 2013 and (b) winter 2016 and 2018. The solid yellow arrow represents the direction of flow of the surface and central water masses, dashed arrows represent the direction of the intermediate and deep water masses described in Table 2. Circles represent upwelling of different water masses observed on the continental shelf. Thin black contours denote the bathymetry (m).

ing velocities are very reliable in this region and note that the mooring data reveals equatorward flow of NADW during both the summer and winter seasons, with more equatorward flow observed during winter (Figure 8).

We find that the strongest seasonal signals within the Agulhas Current are related to mixed layer and submesoscale processes. These deserve a closer look. In particular, the waters over the African shelf and slope need to be measured at higher horizontal resolution to capture the inshore front of the Agulhas Current and the upwelling which have scales of order 20 km and less.

21699291, 2022, 9, Downloaded from https://agupubs.onlinelibrary.wiley.com/doi/10.1029/2021JC018107 by Cochrane France, Wiley Online Library on [12/10/2022]. See the Terms and Conditions (https://onlinelibrary.wiley.com/terms-and-conditions) on Wiley Online Library for rules of use; OA articles are governed by the applicable Creative Commons License

21699291, 2022, 9, Downloaded from https://agupubs.onlinelibrary.wiley.com/doi/10.1029/2021JC018107 by Cochrane France, Wiley Online Library on [12/10/2022]. See the Terms and Conditions (https://onlinelibrary.wiley.com/terms-and-conditions) on Wiley Online Library for rules of use; OA articles are governed by the applicable Creative Commons License

Data Availability Statement

All data used in this study are publically available. The MODIS-AQUA sea surface temperature data is available on the Physical Oceanography Distributed Active Archive Center Drive at https://podaac-tools.jpl.nasa.gov/drive/files/allData/modis/L3/aqua/4um/v2019.0/4km (Physical Oceanography Distributed Active Archive Center, 2021). And the gridded maps of Absolute Dynamic Topography were freely extracted from the Copernicus Marine Service at https://resources.marine.copernicus.eu/product-detail/SEALEVEL_GLO_PHY_L4_REP_OBSERVATIONS_008_047/INFORMATION (Copernicus Marine Service, 2021). The hydrographic data from the Agulhas System Climate Array (ASCA) surveys (Hermes et al., 2021) are available from the South African Environmental Observation Network data portal at https://catalogue.saeon.ac.za/records whereas the hydrographic data from the ACT surveys can (Beal, 2021) be found online at the CLIVAR and Carbon Hydrographic Data Office at http://cchdo.ucsd.edu. The Agulhas Current transport proxy (Beal & Elipot, 2016a, 2016b,) is based on a relationship between satellite sea surface height and in situ current meter measurements from the Agulhas Current Time-series experiment and can be downloaded at https://beal-agulhas.rsmas.miami.edu/data-and-products/index.html. Gridded cross-sectional velocities, temperatures, and salinities are based on in situ current meter measurements from the ASCA experiment (Gunn et al., 2020; McMonigal et al., 2020) and can be downloaded at https://beal-agulhas.rsmas.miami.edu/data-and-products/index.html (Beal Lab, 2020). The MATLAB scripts used for data analysis in this study are published on Zenodo at http://doi.org/10.5281/zenodo.6548374 (Braby & Novelli, 2021).

Acknowledgments

We thank the reviewers for their constructive feedback and role in improving our study. This work was supported by the Department of Science and Innovation, the National Research Foundation and the Department of Forestry, Fisheries and Environment of South Africa. LMB was supported by the US National Science Foundation, Award 1459543. We acknowledge Shane Elipot and Kathryn Gunn for their assistance with processing the CTD and S-ADCP data, as well as Kay McMonigal, Jordan van Stavel, and Tahlia Henry for carefully running salinity samples for calibration of the CTD data. We thank the Captain and crew of the SA Agulhas II, as well as the SEAmester science teams, for their invaluable roles on each of the surveys.

References

Barlow, R., Lamont, T., Britz, K., & Sessions, H. (2013). Mechanisms of phytoplankton adaptation to environmental variability in a shelf ecosystem. *Estuarine, Coastal and Shelf Science*, *133*, 45–57. https://doi.org/10.1016/j.ecss.2013.08.006

Barlow, R., Lamont, T., Kyewalyanga, M., Sessions, H., & Morris, T. (2010). Phytoplankton production and physiological adaptation on the southeastern shelf of the Agulhas ecosystem. *Continental Shelf Research*, *30*(13), 1472–1486. https://doi.org/10.1016/j.csr.2010.05.007

Beal, L. M. (2021). Conductivity temperature depth (CTD) data from 316N20130213, 318M20111103, 316N20100404 ACT cruises. [Data Set]. http://cchdo.ucsd.edu

Beal, L. M., & Bryden, H. L. (1997). Observations of an Agulhas undercurrent. *Deep Sea Research Part I: Oceanographic Research Papers*, *44*(9–10), 1715–1724. https://doi.org/10.1016/S0967-0637(97)00033-2

Beal, L. M., & Bryden, H. L. (1999). The velocity and vorticity structure of the Agulhas Current at 32 S. *Journal of Geophysical Research*, *104*(C3), 5151–5176. https://doi.org/10.1029/1998JC900056

Beal, L. M., Chereskin, T. K., Lenn, Y. D., & Elipot, S. (2006). The sources and mixing characteristics of the Agulhas Current. *Journal of Physical Oceanography*, *36*(11), 2060–2074. https://doi.org/10.1175/JPO2964.1

Beal, L. M., De Ruijter, W. P., Biastoch, A., Zahn, R., Cronin, M., Hermes, J., et al. (2011). On the role of the Agulhas system in ocean circulation and climate. *Nature*, *472*(7344), 429–436. https://doi.org/10.1038/nature09983

Beal, L. M., & Elipot, S. (2016a). Broadening not strengthening of the Agulhas Current since the early 1990s. *Nature*, *540*(7634), 570–573. https://doi.org/10.1038/nature19853

Beal, L. M., & Elipot, S. (2016b). Agulhas current transport proxy data. [Data set]. https://beal-agulhas.rsmas.miami.edu/data-and-products/index.html

Beal, L. M., Elipot, S., Houk, A., & Leber, G. M. (2015). Capturing the transport variability of a western boundary jet: Results from the Agulhas current time-series experiment (ACT). *Journal of Physical Oceanography*, *45*(5), 1302–1324. https://doi.org/10.1175/JPO-D-14-0119.1

Beal Lab. (2020). Agulhas System Climate Array (ASCA)gridded cross-sectional velocity, temperaturs and salinity data. [Data Set]. Retrieved from https://beal-agulhas.rsmas.miami.edu/data-and-products/index.html

Beckley, L. E., & Van Ballegooyen, R. C. (1992). Oceanographic conditions during three ichthyoplankton surveys of the Agulhas Current in 1990/91. *South African Journal of Marine Science*, *12*(1), 83–93. https://doi.org/10.2989/02577619209504693

Biastoch, A., Reason, C. J. C., Lutjeharms, J. R. E., & Boebel, O. (1999). The importance of flow in the Mozambique channel to seasonality in the greater Agulhas Current system. *Geophysical Research Letters*, *26*(21), 3321–3324. https://doi.org/10.1029/1999GL002349

Braby, L., & Novelli, G. (2021). MATLAB scripts for analyzing SEAmester CTD and ADCP data. Version 1.0. *Zenodo*. https://doi.org/10.5281/zenodo.6548374

Carr, M., Lamont, T., & Krug, M. (2021). Satellite sea surface temperature product comparison for the southern African marine region. *Remote Sensing*, *13*(7), 1244. https://doi.org/10.3390/rs13071244

Copernicus Marine Service. (2021). Global ocean gridden L4 sea surface heights and derived variables reprocessed. [Data Set]. Retrieved from https://resources.marine.copernicus.eu/product-detail/SEALEVEL_GLO_PHY_L4_REP_OBSERVATIONS_008_047/INFORMATION

de Boyer Montégut, C., Madec, G., Fischer, A. S., Lazar, A., & Iudicone, D. (2004). Mixed layer depth over the global ocean: An examination of profile data and a profile-based climatology. *Journal of Geophysical Research*, *109*(C12), C12003. https://doi.org/10.1029/2004JC002378

Elipot, S., Beal, L. M., Houk, A., & Leber, G. M. (2015). Characteristics, energetics, and origins of Agulhas Current meanders and their limited influence on ring shedding. *Journal of Physical Oceanography*, *45*(9), 2294–2314. https://doi.org/10.1175/JPO-D-14-0119.1

Gill, A. E., & Schumann, E. H. (1979). Topographically induced changes in the structure of an inertial coastal jet: Application to the Agulhas current. *Journal of Physical Oceanography*, *9*(5), 975–991. https://doi.org/10.1175/1520-0485(1979)009<0975:TICITS>2.0.CO;2

Gründlingh, M. L. (1985). Occurrence of red sea water in the southwestern Indian ocean, 1981. *Journal of Physical Oceanography*, *15*(2), 207–212. https://doi.org/10.1175/1520-0485(1985)015<0207:OORSWI>2.0.CO;2

Gunn, K. L., Beal, L. M., Elipot, S., McMonigal, K., & Houk, A. (2020). Mixing of subtropical, central, and intermediate waters driven by shifting and pulsing of the Agulhas Current. *Journal of Physical Oceanography*, *50*(12), 3545–3560. https://doi.org/10.1175/JPO-D-20-0093.1

Hermes, J., Ansorge, I., Beal, L., Elipot, S., Duncombe-Rae, C., & Ridderinkhof, K. (2021). The ASCA April 2015, July 2016, January 2018, July 2018, July 2019 conductivity temperature depth (CTD) and acoustic Doppler current profiler (ADCP) data [Data Set]. South African Environmental Observation Network. https://catalogue.saeon.ac.za/records .

Hutchings, L. (1994). The Agulhas bank: A synthesis of available information and a brief comparison with other east-coast shelf regions. *South African Journal of Science*, *90*(3), 179–185.

Hutchinson, K., Beal, L. M., Penven, P., Ansorge, I., & Hermes, J. (2018). Seasonal phasing of Agulhas current transport tied to a baroclinic adjustment of near-field winds. *Journal of Geophysical Research: Oceans*, *123*(10), 7067–7083. https://doi.org/10.1029/2018JC014319

Krug, M., & Tournadre, J. (2012). Satellite observations of an annual cycle in the Agulhas Current. *Geophysical Research Letters*, *39*(15). https://doi.org/10.1029/2012GL052335

Lamont, T., Brewin, R. J. W., & Barlow, R. G. (2018). Seasonal variation in remotely-sensed phytoplankton size structure around southern Africa. *Remote Sensing of Environment*, *204*, 617–631. https://doi.org/10.1016/j.rse.2017.09.038

Leber, G. M., & Beal, L. M. (2014). Evidence that Agulhas Current transport is maintained during a meander. *Journal of Geophysical Research: Oceans*, *119*(6), 3806–3817. https://doi.org/10.1002/2014JC009802

Leber, G. M., & Beal, L. M. (2015). Local water mass modifications by a solitary meander in the Agulhas Current. *Journal of Geophysical Research: Oceans*, *120*(6), 4503–4515. https://doi.org/10.1002/2015JC010863

Leber, G. M., Beal, L. M., & Elipot, S. (2017). Wind and current forcing combine to drive strong upwelling in the Agulhas Current. *Journal of Physical Oceanography*, *47*(1), 123–134. https://doi.org/10.1175/JPO-D-16-0079.1

Lutjeharms, J. R. (2006). *The Agulhas current* (Vol. 329). Springer.

Lutjeharms, J. R. E., Cooper, J., & Roberts, M. (2000). Upwelling at the inshore edge of the Agulhas current. *Continental Shelf Research*, *20*(7), 737–761. https://doi.org/10.1016/S0278-4343(99)00092-8

Matano, R. P., Beier, E. J., Strub, P. T., & Tokmakian, R. (2002). Large-scale forcing of the Agulhas variability: The seasonal cycle. *Journal of Physical Oceanography*, *32*(4), 1228–1241. https://doi.org/10.1175/1520-0485(2002)032<1228:LSFOTA>2.0.CO;2

McMonigal, K., Beal, L. M., Elipot, S., Gunn, K. L., Hermes, J., Morris, T., & Houk, A. (2020). The impact of meanders, deepening and broadening, and seasonality on Agulhas Current temperature variability. *Journal of Physical Oceanography*, *50*(12), 3529–3544. https://doi.org/10.1175/JPO-D-20-0018.1

Minnett, P. J., Smith, M., & Ward, B. (2011). Measurements of the oceanic thermal skin effect. *Deep Sea Research Part II: Topical Studies in Oceanography*, *58*(6), 861–868. https://doi.org/10.1016/j.dsr2.2010.10.024

Physical Oceanography Distributed Active Archive Center. (2021). MODIS Aqua level 3 thermal IR daily daytime sea surface temperature from the moderate resolution imaging spectroradiometer (MODIS) on the Aqua satellite from the NASA ocean biology processing group (OBPG). [Data Set]. Retrieved from https://podaac-tools.jpl.nasa.gov/drive/files/allData/modis/L3/aqua/11um/v2019.0/4km

Russo, C. S., Lamont, T., Tutt, G. C. O., van den Berg, M. A., & Barlow, R. G. (2019). Hydrography of a shelf ecosystem inshore of a major western boundary current. *Estuarine, Coastal and Shelf Science*, *228*, 106363. https://doi.org/10.1016/j.ecss.2019.106363

Schumann, E. H. (1982). Inshore circulation of the Agulhas current off natal. *Journal of Marine Research*, *40*(1), 43–55.

Schumann, E. H. (1988). *Physical oceanography off natal* (Vol. 26, pp. 101–130). Coastal Ocean Studies off Natal. https://doi.org/10.1029/LN026p0101

Schumann, E. H. (1999). Wind-driven mixed layer and coastal upwelling processes off the south coast of South Africa. *Journal of Marine Research*, *57*(4), 671–691. https://doi.org/10.1357/002224099321549639

Visbeck, M. (2002). Deep velocity profiling using lowered acoustic doppler current profilers: Bottom track and inverse solutions. *Journal of Atmospheric and Oceanic Technology*, *19*(5), 794–807. https://doi.org/10.1175/1520-0426(2002)019<0794:DVPULA>2.0.CO;2

Yang, D. Z., Huang, R. X., Yin, B. S., Feng, X. R., Chen, H. Y., Qi, J. F., et al. (2018). Topographic beta spiral and onshore intrusion of the Kuroshio Current. *Geophysical Research Letters*, *45*(1), 287–296. https://doi.org/10.1002/2017GL076614

21699291, 2022, 9, Downloaded from https://agupubs.onlinelibrary.wiley.com/doi/10.1029/2021JC018107 by Cochrane France, Wiley Online Library on [12/10/2022]. See the Terms and Conditions (https://onlinelibrary.wiley.com/terms-and-conditions) on Wiley Online Library for rules of use; OA articles are governed by the applicable Creative Commons License